Effective Multi-Path Vector Channel Simulator for Antenna Array Systems

Alex Stéphenne and Benoît Champagne

***Abstract*—In this paper, we present a new, computationally efficient simulator for time-varying multi-path (fast fading) vector channels that can be used to evaluate the performance of antenna array wireless receivers at the base station. The development of the simulator is based on the emulation of the spatio-temporal correlation properties of the vector channel. The channel is modeled as a single-input multi-output finite impulse response (FIR) system with time-varying coefficients which are obtained via the application of a space-time correlation shaping transformation on some independent random sequences. The various parts of the new simulator are detailed and channel simulation realizations are presented and commented.**

I. Introduction

BECAUSE of the limited availability of spectrum, wireless system designers are under pressure to achieve high spectral efficiency. To this end, future wireless systems will almost certainly use adaptive antenna arrays [1], [2]. Since performance analysis of communication systems is often done first via computer simulations, there is a need for an effective multi-path vector (multi-antenna) channel simulator. The design of such a simulator must be done with great care since the performance increase associated with the use of beamforming, space diversity, and/or path diversity for a given simulated system is strongly dependent on the temporal and spatial characteristics of the channel.

To study the performance of antenna array receivers via simulation, it is often assumed for simplicity that the multi-path channel characteristics vary slowly as compared to the symbol duration, so that a fixed vector channel can be used (e.g. [3]–[9]). The main limitation of such an approach is that one can obviously not study the tracking properties of the algorithms used to adapt the receiver filters. Recently, a time-varying vector channel simulator has been presented in [10]. The latter decomposes the channel in its time-varying components due to each of the propagation paths, whether they are temporally differentiable or not[1] . Such a simulator becomes very computationally expensive when the number of propagation paths is large, as can be the case in a typical urban environment. A costly new channel simulator (hardware and software) based on a similar approach has even been recently developed [12] to cope with the enormous amount of computations needed to obtain the time-varying channel coefficients. There is clearly a need to develop a vector channel simulator with reduced computational complexity for urban/suburban environment for which the number of time-indifferentiable subpaths (TISs) per time-differentiable path (TDP) is high.

In this paper, we present a new computationally efficient simulator for time-varying multi-path (fast-fading) vector channels that can be used to evaluate the performance of antenna array wireless receivers at the base station when each TDP can be considered as composed of many TISs and there is no line-of-sight transmission path.

The development of the simulator is based on an innovative approach: the emulation of the joint spatio-temporal correlation properties of the channel. The channel is modeled as a single-input multi-output finite impulse response (FIR) system with time-varying channel coefficients which are obtained via the application of a space-time correlation shaping transformation on some independent random sequences. The new simulator is a multi-channel generalization of the scalar channel presented in [13]. The main advantage of the new simulator, as opposed to the ones presented in [10], [12], is that its computational complexity is now proportional to the number of TDPs, regardless of the number of TISs. Another advantage is that fewer topographical parameters are being feed into the simulator making it less environment dependent.

The structure of the paper is as follow. In Section II, the multi-path vector channel is described. The various components of the vector channel simulator are detailed in Section III. Section IV presents and discusses channel simulation realizations which demonstrate the practicability of the new simulator. Some final remarks are given in the Section V.

II. The Multi-Path Vector Channel

In this section, we present the multi-path wireless vector channel model used in the development of the simulator, starting with the transmission model and continuing with the channel statistical characterization.

A. Transmission Model

We consider the transmission of a signal from mobile to base, i.e., the uplink transmission[2] . We suppose that the mobile has

Manuscript received April 5, 1998; revised September 18, 2000. This work was supported in part by the Natural Sciences and Engineering Research Council of Canada.

The authors are with the INRS-Télécommunications, Montréal, PQ, H5A 1C6 Canada (e-mail: astephenne@dataradio.com; champagne@tsp.ece.mcgill.ca.).

Publisher Item Identifier S 0018-9545(00)10959-4.

[1]In order for two paths to be time-differentiable (resolvable), their relative delay of arrival must be greater than the inverse of the bandwidth of the transmitted signal [11].

[2]Downlink transmission modeling is of less interest since the envelope correlation of received signals between antenna elements at the mobile is very low even for relatively small antenna element separation [16]. A multi-path vector channel simulator would therefore consist of many independent scalar channel simulator.

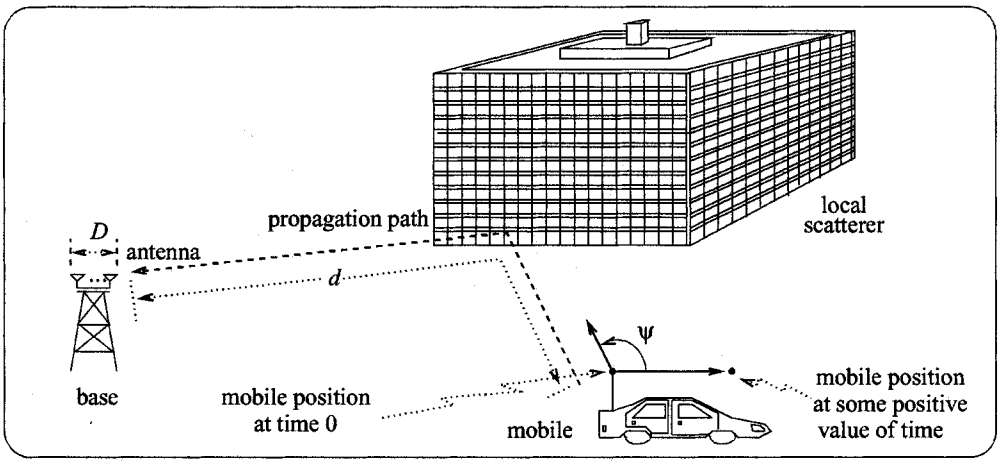

Fig. 1. Illustration of a given transmission path from mobile to base.

a single antenna while an array of antenna elements is used for reception at the base. In order to present the channel model, the following relevant parameters are defined:

- f_c, the carrier frequency ($\omega_c = 2\pi f_c$);
- c, the speed of light;
- λ_c, the carrier wavelength;
- B, the transmitted signal bandwidth;
- v, the speed of the mobile;
- N_e, the number of antenna elements in the array;
- D, the array dimension (the maximum distance between any two arbitrary antenna elements);
- d, the propagation path total length;
- θ, the path angles of arrival (azimuth and elevation) at the antenna array;
- ψ, the Doppler angle associated with a given transmission path;
- $\tau = d/c$, the path propagation delay from mobile to base;
- $\tau_{\min}$ and $\tau_{\max}$, the minimum and maximum propagation delays ($\tau_{\max} = \tau_{\min} +$ delay spread).

Fig. 1 illustrates a given transmission path from the mobile to the antenna array at the base. Note that no specific geometrical restriction on the array configuration is imposed.

The time required for the received waveform associated with a given transmission path to propagate across the array is typically much smaller than the inverse of the transmitted signal bandwidth ($D \ll c/B$). The narrowband array assumption [14] can therefore be used for many wireless communication systems. As an example, in the case of IS-95 for which $B \approx 1.25$ MHz [15], the above assumption is equivalent to $D \ll 240$ m, and is clearly always satisfied for any micro-diversity scheme. Under the narrowband array assumption, one widely used model [5], [7], [8], [10] for the baseband equivalent of the N_e-dimensional vector channel impulse response is given by

$$\mathbf{g}(t,u) = \sum_{i=0}^{M-1} \delta(t-u-\tau_i)\mathbf{a}_i(t) \tag{1}$$

where

- t observation time at the channel output;
- u time at which the impulse is applied at the input;
- $\delta(\cdot)$ Dirac delta function representing this impulse;
- M number of TDPs;
- τ_i propagation delay for the ith TDP;
- $\mathbf{a}_i(t)$ ith complex path vector.

This complex path vector is related to the antenna geometry and is dependent on the amplitude attenuation and phase distortion induced by the channel at the various antenna elements for all TISs associated with the ith TDP. The elements of the complex path vectors, denoted by $a_{ij}(t)$ for $j = 0, \ldots, N_e - 1$, are called here *channel coefficients*.

To simplify the subsequent statistical analysis of the complex path vectors, we choose to visualize the channel impulse response (1) as a linear superposition of propagation path contributions associated to a continuum of angles of arrival (AOA) θ, Doppler angles ψ, and propagation delays τ. We therefore have

$$\mathbf{a}_i(t) = \int_{\mathcal{T}_i} d\tau \int\int d\theta\, d\psi \alpha(\theta,\psi,\tau)\mathbf{v}(\theta)e^{j(\omega_d t\cos\psi - \omega_c\tau)} \tag{2}$$

where

- $\mathcal{T}_i$ domain of integration of τ for the ith TDP which is equal to $[\tau_{\min} + i/B, \tau_{\min} + (i+1)/B]$;
- $\alpha(\theta,\psi,\tau)$ path magnitude density function with respect to the AOA, Doppler angle, and propagation delay;
- $\omega_d = \omega_c v/c$ radial Doppler frequency ($\omega_d = 2\pi f_d$).

The vector $\mathbf{v}(\theta)$ in (2) is the array propagation vector [14], defined here as

$$\mathbf{v}(\theta) = \left[1, e^{-j\omega_c\rho_1(\theta)}, \ldots, e^{-j\omega_c\rho_{N_e-1}(\theta)}\right]^T \tag{3}$$

where $\rho_j(\theta)$ is the time difference of arrival, between the jth and the 0th antenna elements, of the propagation paths with AOA θ; and the superscript T denotes the transpose operator. The terms $e^{j\omega_d t\cos\psi}$, $\mathbf{v}(\theta)$ and $e^{-j\omega_c\tau}$ in (2) are associated with the Doppler effect, the antenna diversity and the transmission delay from mobile to base, respectively. Note that the array propagation vector definition (3) could be modified to include the effect of antenna element directionality.

It is important to outline the limitations on the validity of our propagation model imposed by the various hypotheses made to obtain (1) and (2). The derivation of the model presented in this section is detailed in Appendix A. Note that, under our modeling assumptions, the Doppler angle associated with a particular TIS is time-invariant. The model is therefore only valid for small mobile displacements or, equivalently, for short periods of time. The propagation model does not allow for significant mobile or scatterers displacement like the model presented in [12]. Also note that, although the delay associated with individual TDP are assumed fixed in time, the effect of propagation delay variations for the TISs are included in the model and express themselves through the Doppler component in the path vectors. The transmitted signal bandwidth, B, is assumed relatively small, so that the Doppler affects only the carrier frequency, and not the modulation bandwidth, for a given TIS. This last assumption is reasonable for most existing systems but may not be for future wideband systems.

In a typical urban/suburban environment we can often assume that all TDPs are composed of a large number of TISs and that the mobile is surrounded by local reflecting structures so that there is no line-of-sight transmission. By the central limit theorem we then find the channel coefficients to be well approximated by circularly complex Gaussian variables [17], i.e., they are characterized by a Rayleigh envelope [16]. The Rayleigh envelope model for multipath fading is widely used and was validated experimentally [16]. Since Gaussian variables are entirely characterized by their first and second order statistics, we can simulate the channel coefficients $a_{ij}(t)$ by generating Gaussian variables that have appropriate mean and correlation. The first and second order statistics of the desired channel coefficients are characterized in the next subsection.

B. Second Order Characterization

We consider a mobile surrounded by local reflecting structures so that there is a large number of indirect transmission paths each of which exhibiting different AOA θ, delay τ, and Doppler angle ψ.

With the considered framework, it is reasonable to use the following modeling assumptions:

1) TISs corresponding to different delays, AOA, or Doppler angles have uncorrelated amplitudes. That is,

$$E[\alpha(\theta,\psi,\tau)\alpha^*(\theta',\psi',\tau')] = \delta(\theta-\theta',\psi-\psi',\tau-\tau')f(\theta,\psi,\tau) \tag{4}$$

where the superscript $*$ denotes the conjugate operator, and $f(\theta,\psi,\tau)$ is the joint power density function. This assumption is intuitively reasonable since propagation paths associated with different AOA, Doppler angles, or transmission delays do not result from the same interactions with the physical environment.

2) The power density function $f(\theta,\psi,\tau)$ is separable in θ, ψ, and τ, i.e.,

$$f(\theta,\psi,\tau) = f_a(\tau)f_b(\psi)f_c(\theta;i) \tag{5}$$

where $f_a(\tau)$, $f_b(\psi)$ and $f_c(\theta;i)$ are the power density function with respect to the delay, the Doppler angle and the AOA for the ith path, respectively. The intuitive validation of this assumption comes from the fact that there is no direct physical relation between the Doppler angle, the propagation delay and the direction of arrival, so that knowledge of θ, ψ or τ does not give any information about the remaining two.

3) The power density function with respect to the Doppler angle, ψ, is uniform since the local scatterers are uniformly distributed around the mobile.

We define

$$F_a(i) = \int_{\tau_{\min}+i/B}^{\tau_{\min}+(i+1)/B} f_a(\tau)\,d\tau \tag{6}$$

which is simply the power fraction associated with the ith path. Typically, a negative exponential distribution is used to describe the power density function with respect to the transmission delays [19], so that one finds

$$F_a(i) = \left[1 - e^{-1/(B\bar{T})}\right] e^{-i/(B\bar{T})} \tag{7}$$

where $\bar{T}$ is the mean delay.

Because of the random phase associated with each individual TIS in a given TDP (due to the different delays of arrival), it is easily shown that the channel coefficients are well modeled by a zero-mean complex variable [18].

To simplify the analysis of the second order statistics, we suppose that $v\tau_{\max} \ll \lambda_c$. This is respected in vehicular technology ($v < 30$ m/s, $\tau_{\max} < 50$ μs) provided $f_c \ll 200$ GHz. Under our modeling assumptions one may show that the cross-correlation matrix of the complex path vectors is given by (see Appendix B)

$$\mathbf{R}_{ij}(t_1,t_2) \triangleq E\left[\mathbf{a}_i(t_1)\mathbf{a}_j^H(t_2)\right], \tag{8}$$

$$= \delta_{ij}J_0(\omega_d\Delta t)F_a(i)\mathbf{R}_{\mathbf{v},i} \tag{9}$$

where

$\Delta t = t_1 - t_2$ time lag;

$J_0(\cdot)$ Bessel function of the first kind and of order 0;

superscript H denotes the Hermitian-transpose operator; and the matrix $\mathbf{R}_{\mathbf{v},i}$; which is called here the spatial correlation matrix for the ith TDP, is given by

$$\mathbf{R}_{\mathbf{v},i} = \int f_c(\theta;i)\mathbf{v}(\theta)\mathbf{v}^H(\theta)\,d\theta. \tag{10}$$

Note that an expression similar to (9) for the complex path vector cross-correlation matrix is given in [5].

The spatial correlation matrix for the ith TDP, $\mathbf{R}_{\mathbf{v},i}$, can be obtained from (10) once the antenna geometry (or equivalently the functions $\rho_j(\theta)$ in (3)), and the power density functions with respect to the AOA $f_c(\theta;i)$, are selected.

The performance of an antenna array receiver is strongly dependent on the level of correlation between the signals received at the various antenna elements. It is therefore of great interest to develop an intuitive understanding for the spatial correlation characteristics of signals received at the antenna array under our modeling assumptions. To do so, we consider an antenna array of two elements spaced D apart. We also introduce a simple

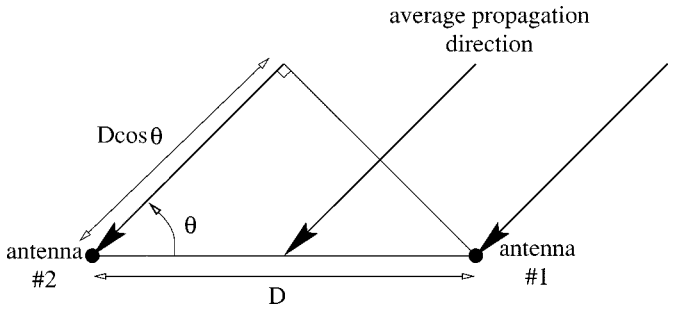

Fig. 2. Geometry of the simple two-elements array model.

propagation model for which all the incoming paths lie in the same plane as the array, and the power density function of the incoming TISs with respect to the angle of arrival is uniform in $\theta \pm \Delta$, where θ is the mean angle of arrival and 2Δ is called the angular spread. The model geometry is illustrated in Fig. 2. Only one TDP (i) is considered. With this model, the spatial correlation matrix $\mathbf{R}_{\mathbf{v},i}$ of (10) is a (2×2) matrix. The spatial correlation between the signals received at the two antenna elements is a function of the antenna separation D, and is simply given by the entry of $\mathbf{R}_{\mathbf{v},i}$ on the second row and first column, denoted by $r(D)$, which is equal to

$$r(D) = \frac{1}{2\Delta} \int_{\theta-\Delta}^{\theta+\Delta} \exp\left(-j2\pi \frac{D}{\lambda_c} \cos\nu\right) d\nu. \quad (11)$$

It can be shown that (11) can be rewritten in the following way:

$$r(D) = J_0\left(2\pi \frac{D}{\lambda_c}\right) + 2\sum_{k=1}^{\infty} (j)^k J_k\left(2\pi \frac{D}{\lambda_c}\right) \cos(k\theta)\mathrm{sinc}(k\Delta/\pi). \quad (12)$$

To a good approximation [16], [19], the envelope correlation is equal to the squared magnitude of the complex signal correlation, so the spatial correlation between the envelopes of the received signals at the two antenna elements, which we denote by $\rho(D)$, is simply given by the squared magnitude of $r(D)$. Figs. 3(a) and (b) illustrate the value of $\rho(D)$ obtained from (12), versus the normalized antenna separation D/λ_c for different values of angular spread and for $\theta = 90°$ (broadside) and $\theta = 20°$, respectively. We note that, as expected, when the angular spread is null $(\Delta = 0)$, maximum spatial envelope correlation exists between the signals at the antenna elements. When $\Delta \neq 0$ and the signal comes from broadside, there are zeros in the spatial correlation at specific values of antenna separation. The larger the angular spread, the lower the value of antenna spacing corresponding to the first zero. When the signal is not coming from broadside, as in Fig. 3(b), the antenna separation necessary for low spatial correlation is larger. In mobile communications, the base is typically far from the mobile and the local scatterers surrounding it, the angular spread induced by these local scatterers, 2Δ, is therefore often relatively small [2], of the order of a few degrees at most. With such values of angular spread, Fig. 3 indicates that the spatial envelope correlation between two antenna array elements can remain relatively high even if they are separated by many λ_c.

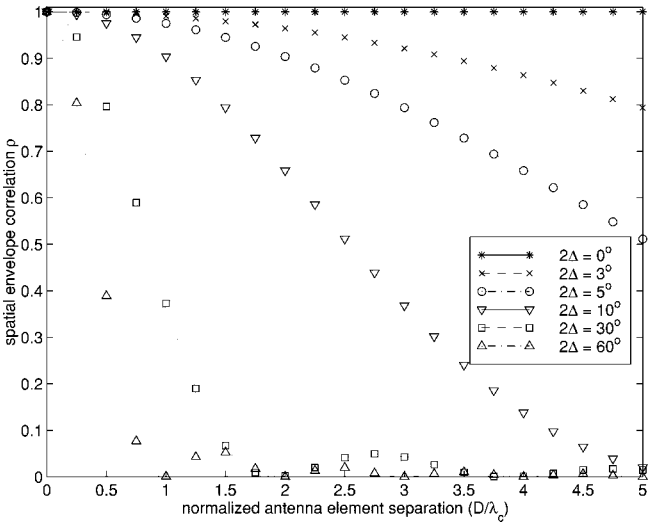

(a)

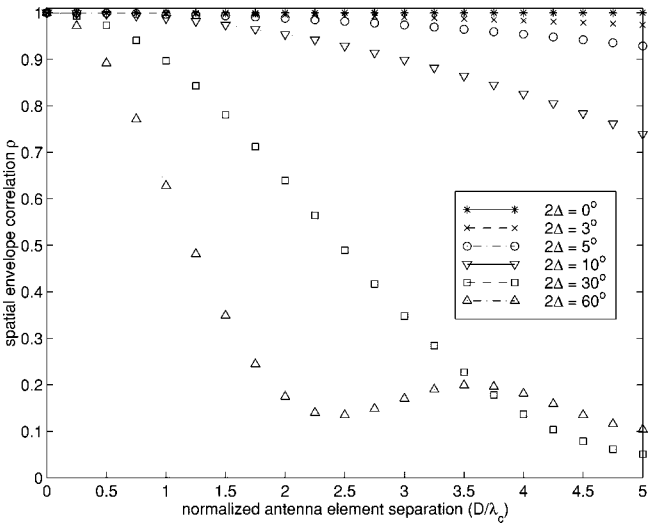

(b)

Fig. 3. Spatial envelope correlation $\rho(D)$ *versus* normalized antenna separation for different values of angular spread and for two values of average angle of arrival. (a) $\theta = 90^{\mathrm{deg}}$. (b) $\theta = 20^{\mathrm{deg}}$

III. New Vectorial Channel Simulator

The new channel simulator is described in this section. The general structure of the simulator is first presented and a detailed description of its main component, the complex path vector generator, is then given.

A. Simulator Structure

The vectorial channel simulator structure is shown in Fig. 4. It is a single-input multi-output discrete-time FIR filter with time-varying coefficients, based on a tapped-delay-line model with evenly spaced taps one sample apart. The time index and the corresponding sampling interval are denoted by k and T_c, respectively. The sampling rate is set equal to the Nyquist rate, i.e., $T_c = 1/B$. The input to the channel simulator, $z(k)$, is the baseband transmitted signal; the outputs, $s_j(k)$ $(j = 0, \ldots, N_e - 1)$ are the baseband received signals at the N_e antenna elements. The ith tap input of the jth tapped-delay-line associated with the jth antenna, i.e., $z(k - i)$, is multiplied by a time-varying

channel coefficient $a_{ij}(k)$. A complex noise signal $n_j(k)$ modeling external noise or possibly multiuser interferences is added to the jth tapped-delay-line output. The power of this noise signal is chosen according to the required signal-to-(interference-plus)-noise ratio.

The vector channel simulator main task is to synthesize the complex path vectors $\mathbf{a}_i(k)$ $(i = 0, \ldots, M-1)$, i.e., the time-varying channel coefficients $a_{ij}(k)$, so that their cross-correlation characteristics are as given by (9). The complex path vector generator used to obtain the desired channel coefficients is described in the next subsection.

B. Complex Path Vector Generator

The basic philosophy behind the complex path vector generator is to devise some kind of space-time correlation shaping transformation that will be applied to uncorrelated Gaussian white noise sequences in order to obtain a discrete-time version of the time-varying complex path vectors $\mathbf{a}_i(t)$ $(i = 0, \ldots, M-1)$ in (1) exhibiting the appropriate spatio-temporal correlation properties, as given by (9). Such a transformation would permit to generalize the scalar channel simulator presented in [13] to the vectorial (multi-channel) case. Note that contrarily to the simulation approach presented in [12], our approach bypass the tracking of high resolution delays for the TISs by stochastically modeling the channel variations due to the Doppler effect. These channel variations are narrowband by nature so that their tracking can be done at a relatively low rate.

As shown later on, as long as the complex path vectors are obtained at a rate higher than twice the Doppler frequency, their temporal correlation structure is preserved when interpolation procedures are used, later on, to bring the sampling rate to a higher value. Since the Doppler frequency is typically much smaller than B, it is computationally profitable to do the digital processing required to obtain the complex path vectors at a smaller rate than the rate $1/T_c = B$ used in Fig. 4. The complex path vectors obtained at this reduced rate, which we denote by $1/T$, can then be interpolated to the higher required rate $1/T_c$.

Observation of (9) indicates that the complex path vectors are independent, which means that the simulated channel coefficients can be generated independently for each TDP. Furthermore, by rewriting (9) in the following way for the case $i = j$:

$$\mathbf{R}_{ii}(\Delta t) = J_0(\omega_d \Delta t)\mathbf{C}_i \tag{13}$$

where

$$\mathbf{C}_i = F_a(i)\mathbf{R}_{\mathbf{v},i} \tag{14}$$

we note that the matrix $\mathbf{C}_i$ is independent of Δt. This suggests that, in order to obtain the appropriate space-time correlation characteristics for a given path, one can use a time transformation followed by a spatial transformation. More precisely, the desired time-varying complex path vector for the ith TDP $\mathbf{a}_i(k)$, which is used in Fig. 4, can be obtained from the complex path vector generator illustrated in Fig. 5.

The time index m in Fig. 5 refers to the sampling interval of the complex path vectors prior to interpolation, which is denoted by T. The noise generator to the left of Fig. 5 produces zero-mean circularly complex Gaussian vectors

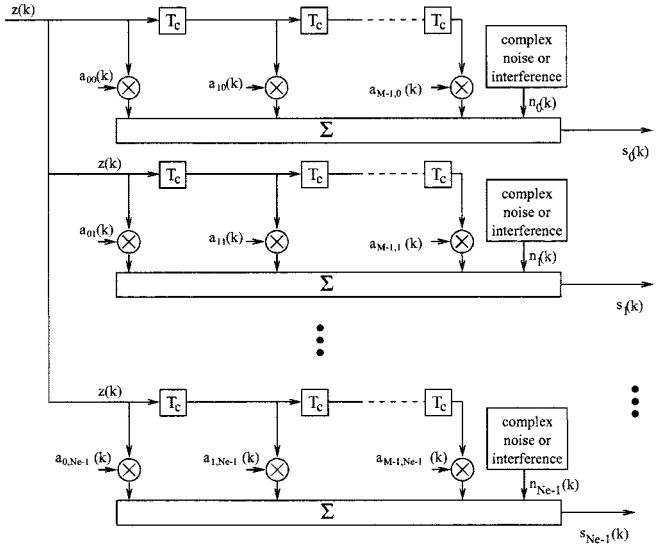

Fig. 4. Time-varying vector channel simulator.

$$\tilde{\mathbf{n}}_i(m) = [\tilde{n}_{i0}(m) \quad \tilde{n}_{i1}(m) \quad \cdots \quad \tilde{n}_{i,N_e-1}(m)]^T \tag{15}$$

such that

$$E\left[\tilde{\mathbf{n}}_i(m)\tilde{\mathbf{n}}_i^H(l)\right] = \mathbf{I}\delta_{ml}. \tag{16}$$

The time-correlation shaping filter (TCSF) denoted by $H(z)$ in Fig. 5 is designed so that the temporal correlation of its output, $y_{ij}(m) = H(z)\tilde{n}_{ij}(m)$, is approximately equal to the temporal component in (13), namely $J_0(\omega_d \Delta t)$. Note that the same TCSF will be used for each TDP since the time-correlation component in (13) is independent of the TDP index i. Section III–B1 is devoted to the design of the required TCSF.

The space-correlation shaping transformation in Fig. 5 takes care of the spatial component of the correlation, i.e., $\mathbf{C}_i$ in (13). This transformation is applied to the vector $\mathbf{y}_i(m)$ whose entries are the output of the time shaping filters (one for each antenna elements) at time m for the ith TDP, i.e.,

$$\mathbf{y}_i(m) = [y_{i0}(m) \quad y_{i1}(m) \quad \cdots \quad y_{i,N_e-1}(m)]^T. \tag{17}$$

Section III-B2 gives all the details on how to obtain the space-correlation shaping transformation.

By combining a properly designed TCSF and spatial transformation, we end up with a procedure for synthesizing time-varying complex path vectors with the desired space-time correlation properties. The obtained simulated complex path vectors are finally interpolated in time to the desired sampling rate $1/T_c = B$.

A more detailed description of the various components of the complex path vector generator of Fig. 5 will now be given.

1) Time-Correlation Shaping Filter (TCSF): The use of a TCSF to obtain the desired temporal correlation is not a new approach. It was already used more than twenty years ago [20], and was still used recently [13]. The desired power spectral den-

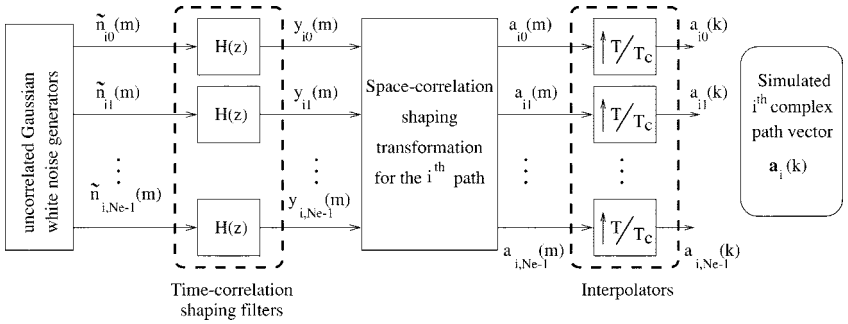

Fig. 5. Structure of the complex path vector generator (one such structure per TDP i).

sity function, denoted by $\mathcal{S}(\omega)$, is the Fourier transform of the Bessel function in (13), and is given by

$$\mathcal{S}(\omega) = \begin{cases} \frac{2}{\sqrt{\omega_d^2 - \omega^2}} & \text{if } |\omega| \leq \omega_d, \\ 0 & \text{otherwise.} \end{cases} \tag{18}$$

The Fig. 6 illustrates $\mathcal{S}(\omega)$ versus normalized frequency (normalized by the sampling frequency $1/T$ characterized below). For the optimal TCSF, we have $|H(e^{j\omega})|^2 = \mathcal{S}(\omega)$ and the impulse response is infinite in length. But since $\mathcal{S}(\omega)$ has singularities at $\omega = \pm\omega_d$, the design of a stable TCSF with $|H(e^{j\omega})|^2 = \mathcal{S}(\omega)$ is unrealizable. In practice, the singularities around $\omega = \pm\omega_d$ are replaced by sharp peaks. If a FIR filter is selected to approximate the optimal TCSF, as in [20], the order of the filter must be high to obtain a sharp frequency response. To reduce computational complexity, a low order infinite impulse response (IIR) filter was used in [13]. No design details for the TCSF are given in this reference. It is only said that a second-order biquadratic filter with a very low damping factor is used. For this reason, a new IIR TCSF design is presented in this section.

The new TCSF is linear and time invariant. The associated impulse response and its z-transform are denoted by $h(m)$ and $H(z) = \sum_{m=0}^{\infty} h(m) z^{-m}$, respectively. The sampling rate $1/T$ must be high enough so that the temporal correlation structure of the channel coefficients is preserved when interpolation procedures are used, later on, to bring the sampling rate to its desired value $1/T_c$. To do so, the selected value of $1/T$ must be higher than the Nyquist frequency [21] which is twice the Doppler frequency f_d. We selected $1/T = 3/2 \times 2f_d$. A pole-zero TCSF of order K

$$H(z) = \frac{\sum_{k=0}^{K} b_i z^{-i}}{\sum_{k=0}^{K} a_i z^{-i}} \tag{19}$$

is considered. To obtain the $\{a_i\}$ and $\{b_i\}$, we consider the minimization of an error function via a BFGS quasi-Newton method [22]. The selected error function, $J(\{a_i\}, \{b_i\})$, is given by

$$J(\{a_i\}, \{b_i\}) = \sum_{l=0}^{L-1} [\mathcal{S}(\omega_l) - |H(e^{j\omega_l})|^2]^2 \tag{20}$$

where the $\{\omega_l\}$ are L frequency samples uniformly distributed in $[0, 2\pi)$. The minimization procedure was repeated for various values of filter order $K = 1, 2, 4, 6, 8$ and number of frequency points $L = 128\,256\,512$. Since $f_d = T/3$, by taking values of L which are not divisible by three, the singularities of $\mathcal{S}(\omega)$ at $\omega = \pm\omega_d$ pose no problem since they are not considered in the minimization process. A good compromise between complexity and performance was achieved with $K = 4$ and $L = 256$. The obtained coefficients of $H(z)$ are given in Table I. The desired and obtained power spectral density $\mathcal{S}(\omega)$ and $|H(e^{j\omega})|^2$ are illustrated in Fig. 6. A pole-zero diagram for the new TCSF is given in Fig. 7, while the first hundred samples of the TCSF impulse response are plotted in Fig. 8. The temporal correlation of the TCSF output, $y_{ij}(m) = H(z)\tilde{n}_{ij}(m)$, and the desired temporal correlation, $J_0(\omega_d \Delta t)$ are illustrated in Fig. 9.

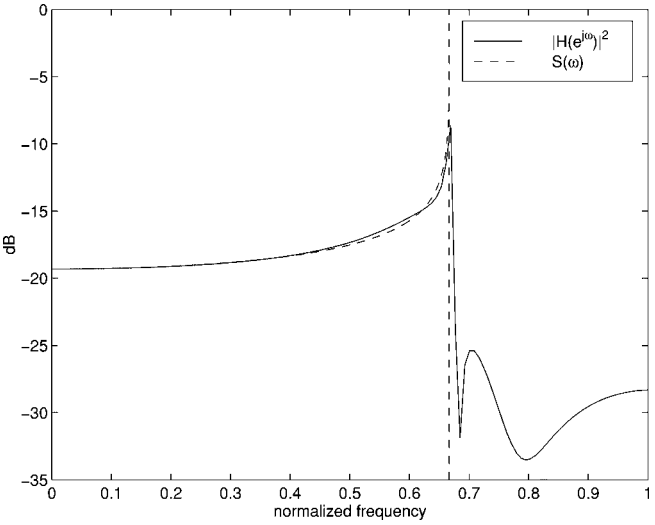

Fig. 6. Desired and obtained power spectral density functions $\mathcal{S}(\omega)$ and $|H(e^{j\omega}|^2$.

2) Spatial Transformation: The spatial transformation used to obtain the complex path vector $\mathbf{a}_i(m)$ from $\mathbf{y}_i(m)$ (17) is a linear and memoryless operator. It takes the form of a simple matrix multiplication, i.e.,

$$\mathbf{a}_i(m) = \mathbf{M}_i \mathbf{y}_i(m). \tag{21}$$

From (8), (9), (13), and (21), we can see that one must find a matrix $\mathbf{M}_i$ such that $\mathbf{M}_i \mathbf{M}_i^H = \mathbf{C}_i$.

The development of the spatial transformation operator $\mathbf{M}_i$ is based on the Karhunen-Loève expansion for vectorial random processes [23], [17]. Since the matrix $\mathbf{C}_i$ is the correlation matrix of a discrete-time stochastic process, it is a nonnegative definite Hermitian matrix [17]. Any Hermitian matrix is diagonalizable [17], so that we can write

$$\mathbf{C}_i = \mathbf{Q}_i \mathbf{\Lambda}_i \mathbf{Q}_i^H \tag{22}$$

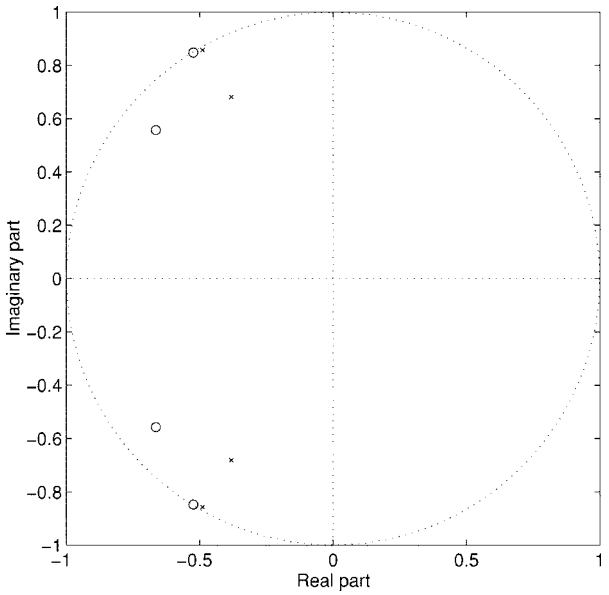

Fig. 7. Pole-zero diagram of the obtained TCSF.

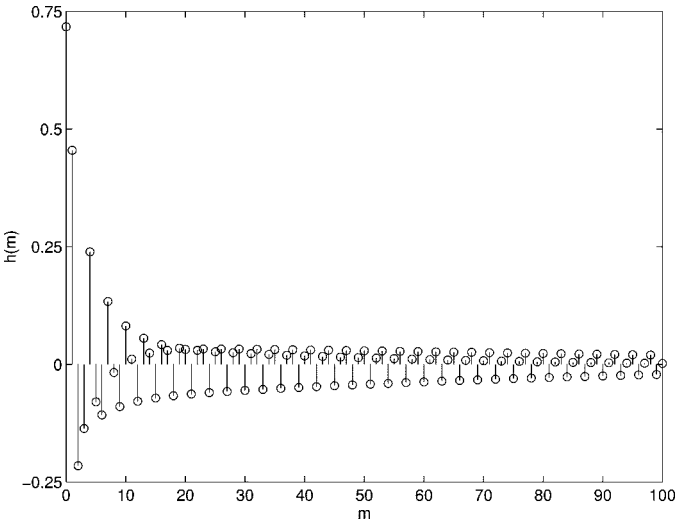

Fig. 8. First samples of the impulse response $h(m)$.

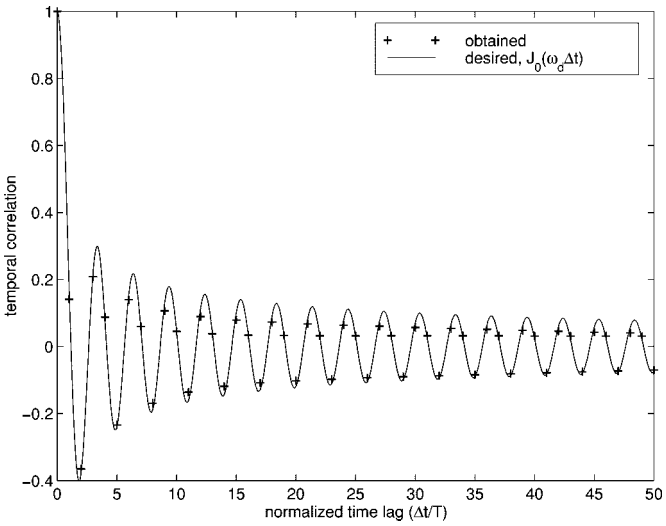

Fig. 9. Desired and obtained temporal correlations.

TABLE I
$H(z)$ COEFFICIENTS OBTAINED VIA OPTIMIZATION

i	a_i	b_i
0	1	0.71724504566570
1	1.74287599025769	1.70502826332690
2	2.33391801449333	2.25142875250905
3	1.34276412323384	1.51287592873974
4	0.59552189482577	0.53630149817269

where $\mathbf{Q}_i$ the matrix whose columns are the orthonormalized eigenvectors of $\mathbf{C}_i$, denoted by $\mathbf{q}_{ij}$ $(j = 0, \ldots, N_e - 1)$, and $\mathbf{\Lambda}_i$ is the diagonal matrix whose entries are the corresponding eigenvalues λ_{ij}. Note that the premultiplication of a vector by $\mathbf{Q}_i$ represents an orthogonal transformation from the $\{\mathbf{q}_{i0}, \ldots, \mathbf{q}_{i,N_e-1}\}$ basis to the canonical basis. Of course the premultiplication of a vector by $\mathbf{Q}_i^H = \mathbf{Q}_i^{-1}$ does the inverse transformation. The fact that $\mathbf{C}_i$ is nonnegative definite implies that $\mathbf{q}_{ij}^H \mathbf{C}_i \mathbf{q}_{ij} \geq 0$, but since, by definition, $\mathbf{C}_i \mathbf{Q}_i = \mathbf{Q}_i \mathbf{\Lambda}_i$, or equivalently $\mathbf{C}_i \mathbf{q}_{ij} = \lambda_{ij} \mathbf{q}_{ij}$, we have $\mathbf{q}_{ij}^H \mathbf{C}_i \mathbf{q}_{ij} = \lambda_{ij} \|\mathbf{q}_{ij}\|^2 = \lambda_{ij} \geq 0$, so that the eigenvalues of $\mathbf{C}_i$ are real and nonnegative. We can therefore write

$$\mathbf{C}_i = \mathbf{Q}_i \mathbf{\Lambda}_i^{1/2} \mathbf{\Lambda}_i^{1/2} \mathbf{Q}_i^H \tag{23}$$

$$= \left[\mathbf{Q}_i \mathbf{\Lambda}_i^{1/2}\right] \left[\mathbf{Q}_i \mathbf{\Lambda}_i^{1/2}\right]^H \tag{24}$$

$$= \mathbf{M}_i \mathbf{M}_i^H \tag{25}$$

where $\mathbf{M}_i = \mathbf{Q}_i \mathbf{\Lambda}_i^{1/2}$ is the desired matrix used in the spatial transformation (21).

Premultiplication of the spatially uncorrelated signal vector $\mathbf{y}_i$ by $\mathbf{M}_i = \mathbf{Q}_i \mathbf{\Lambda}_i^{1/2}$ gives a complex path vector $\mathbf{a}_i(m)$ such that

$$E\left[\mathbf{a}_i(m)\mathbf{a}_i^H(k)\right] = \mathbf{Q}_i \mathbf{\Lambda}_i^{1/2} E\left[\mathbf{y}_i(m)\mathbf{y}_i^H(k)\right] \mathbf{\Lambda}_i^{1/2} \mathbf{Q}_i^H \tag{26}$$

$$\approx \mathbf{Q}_i \mathbf{\Lambda}_i^{1/2} J_0(\omega_d T(k-m)) \mathbf{\Lambda}_i^{1/2} \mathbf{Q}_i^H \tag{27}$$

$$\approx J_0(\omega_d T(k-m)) \mathbf{Q}_i \mathbf{\Lambda}_i \mathbf{Q}_i^H \tag{28}$$

$$\approx J_0(\omega_d T(k-m)) \mathbf{C}_i \tag{29}$$

which is the desired result (13). The approximation made in going from (26) to (27) simply comes from the fact that the designed TCSF $H(z)$ gives a vector $\mathbf{y}_i(m)$ whose elements have a temporal correlation which is not exactly equal to $J_0(\omega_d T(k-m))$ (see Fig. 9).

Fig. 10 illustrates the space-correlation transformation for the ith path. Each element $y_{ij}(m)$ of the spatially uncorrelated signal vector $\mathbf{y}_i$ (from the output of the TCSF) is first scaled by the square root of the eigenvalue λ_{ij}. The resulting vector is then premultiplied by the eigenvector matrix $\mathbf{Q}_i$. The output of the path vector generator, $\mathbf{a}_i(m)$ $(i = 0, \ldots, M-1)$, has the appropriate time-space correlation properties.

Note that if the angular spread associated with a given TDP i is small (of the order of a few degrees) and the number of an-

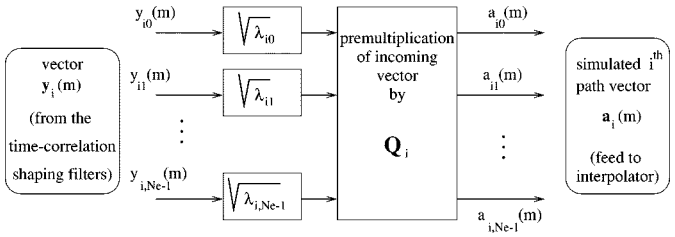

Fig. 10. Space-correlation shaping transformation.

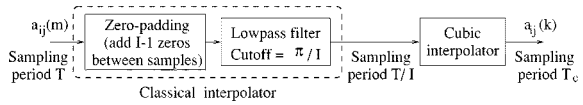

Fig. 11. General system for interpolation.

tenna elements N_e is high, then a few of the associated eigenvalues λ_{ij} $(j = 0, \ldots, N_e - 1)$ will dominate the others in amplitude [24]. It is therefore possible, under these conditions, to reduce the computational requirements of the spatial transformation by setting the small eigenvalues to zero.

It is important to mention that the space-correlation shaping transformation of Fig. 10 can be used independently of the vector channel simulator presented in this paper to obtain sequences with the appropriate spatial correlation from mutually uncorrelated sequences that already exhibit the appropriate temporal correlation. Such sequences could have been obtain previously from scalar channel simulators such as those presented in [16], or could simply be temporally uncorrelated sequences if for a given application one needs to generate a simulated channel exhibiting no temporal correlation between observations.

3) Interpolator: As said earlier, the sampling frequency associated with the channel filtering $1/T_c = B$ is typically much larger than the one associated with the complex path vector generator $1/T = 3f_d$ (see Figs. 4 and 5). We therefore need to obtain the high rate channel coefficients $a_{ij}(k)$ required for channel filtering from the low rate ones $a_{ij}(m)$ via interpolation. When a signal with a sampling frequency much higher than the Nyquist frequency has to be interpolated, simple methods such as linear or cubic interpolation can be used without compromising on the precision [25]. In our case, the sampling frequency $1/T_c$ is typically much larger than $1/T$, which is $3/2$ the Nyquist frequency associated with the channel coefficients. It is therefore possible to decompose the interpolation process to reduce computational requirements. To do so, we use the interpolation system shown in Fig. 11. The system is composed of a classical interpolator [26] followed by a cubic interpolator [25]. The classical interpolator increases by a factor I of at least 30 the sampling rate which becomes much higher than the Nyquist frequency. It does so by adding $I - 1$ zeros between samples (zero-padding) and filtering the resulting signal with a low-pass filter that has a radial cutoff frequency of π/I. Once the classical interpolation is done, a computationally less intensive cubic interpolator is being used to further increase the sampling frequency to its desired value $1/T_c$. The total system is much less computationally demanding than would be a classical interpolator alone. Note that if the mobile speed is null, i.e., $v = 0$, $T = 1/(3f_d)$ becomes infinite and no interpolation (or TCSF) is required since a time-invariant simulated channel is obtained.

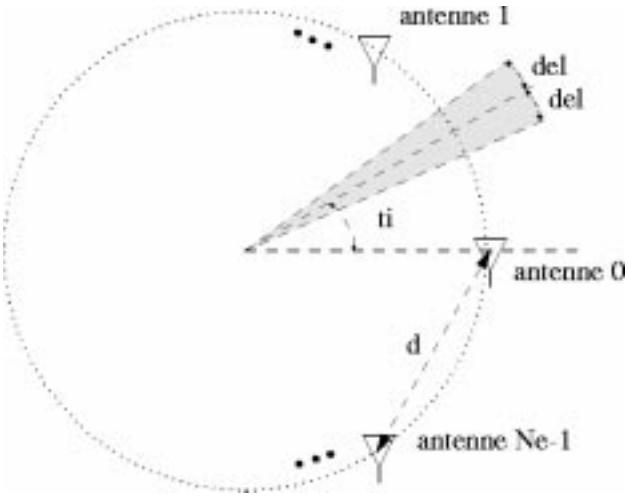

Fig. 12. Geometry of the antenna array and of a given TDP, i (top view).

TABLE II
PATH ANGLE OF ARRIVAL PARAMETERS

	$i = 0$	$i = 1$	$i = 2$
mean angle, θ_i (degrees)	90	150	270
angle spread, $2\Delta_i$ (degrees)	5	10	2

IV. SIMULATION EXAMPLE

In this section, we present and analyze a channel realization obtained with the new time-varying vector channel simulator described above.

In this example, we consider $M = 3$ TDPs and a horizontal circular array of $N_e = 7$ receiving antenna elements separated by half a wavelength. To simplify the analysis of the directivity of the channel we assume that all the propagation paths lie in the same plane as the array (elevation angle is null), and that the power density function with respect to the azimuth angle for the ith TDP is uniform in the interval $\theta_i \pm \Delta_i$, where θ_i is the mean angle of arrival and $2\Delta_i$ is the angular spread for the ith path. The geometry of the antenna array and of a given TDP, i, is given in Fig. 12. Note that a far-field assumption is used, so that the angle of arrival for a given TIS is the same at any position on the antenna array.

In our example, $\theta_0 = 90°$, $\theta_1 = 150°$, $\theta_2 = 270°$, $\Delta_0 = 2.5°$, $\Delta_1 = 5°$, and $\Delta_2 = 1°$. These parameters are displayed in Table II for quick reference. The selected mobile speed is 30 m/s (108 km/h), the carrier frequency f_c is 1 GHz (Doppler frequency $f_d = 100$ Hz), the transmitted signal bandwidth B is 1.2288 MHz, the negative exponential delay profile is used and the mean delay $\bar{T}$ in (7) is set to $\bar{T} = 2/B = 2T_c$. The complex path vector update interval is $T = 1/(3f_d) = 4096T_c$ before interpolation. The classical interpolation decreases this interval to $128T_c$ ($I = 32$ in Fig. 11) while the cubic interpolator brings it down from $128T_c$ to T_c.

Fig. 13 illustrates the evolution in time of the magnitude of the channel coefficients for antenna element 0, i.e., $a_{i0}(k)$ for

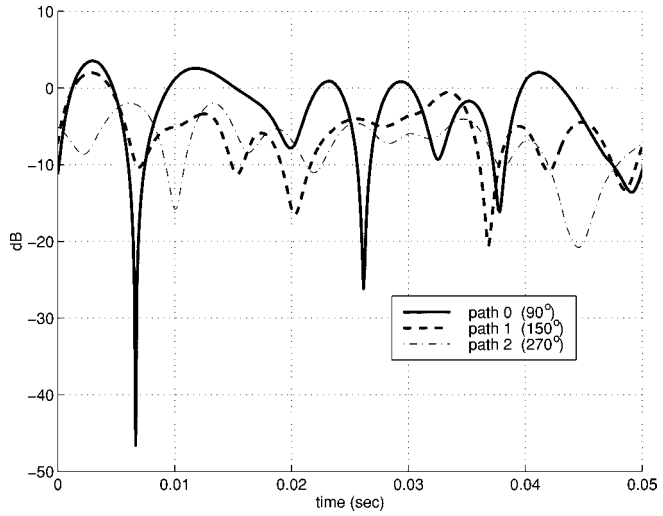

Fig. 13. Channel coefficient magnitudes *versus* time for antenna element 0.

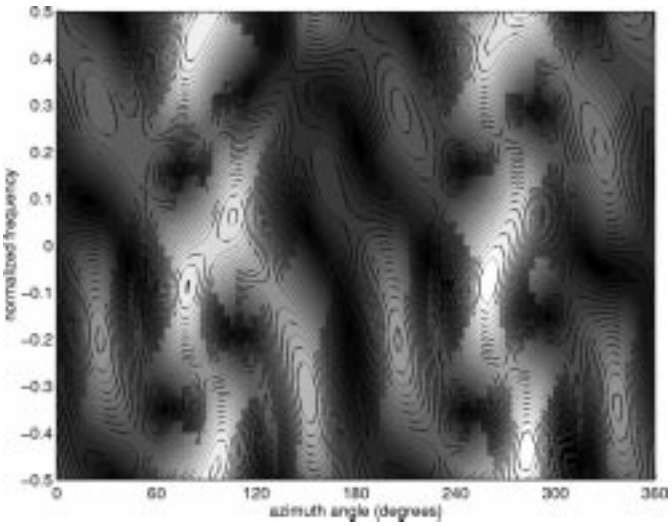

Fig. 14. Directivity pattern (contour plot) for receiver matched to simulated channel at $t = 0.02$ s.

$i = 0, 1, 2$. Due to the fact that there is high channel coefficients correlation between antennas, the evolution in time of the channel coefficients for the two other antennas is almost identical and is therefore not shown. Comparing the shapes of the curves in Fig. 13 with what is shown in the literature (in [27] for example), we see that the time evolution of the simulated channel coefficients is representative of a typical wireless channel.

Next, we show that channel coefficients with appropriate spatial characteristics are being obtained by the new channel simulator. To this end, we look at the directivity pattern (DP) of a receiver matched to the simulated channel, i.e., a receiver whose coefficients are simply the complex conjugate of the channel coefficients. The DP is simply a graph of the gain of the receiver *versus* the azimuth angle (and frequency if the frequency is not set to a particular value) of the incoming paths. A DP contour plot at time $t = 0.02$ s for all possible values of normalized frequency and azimuth angle is shown in Fig. 14. The brighter the region in this figure, the higher the gain of the receiver. We can see that, as expected, most of the incoming energy arrives

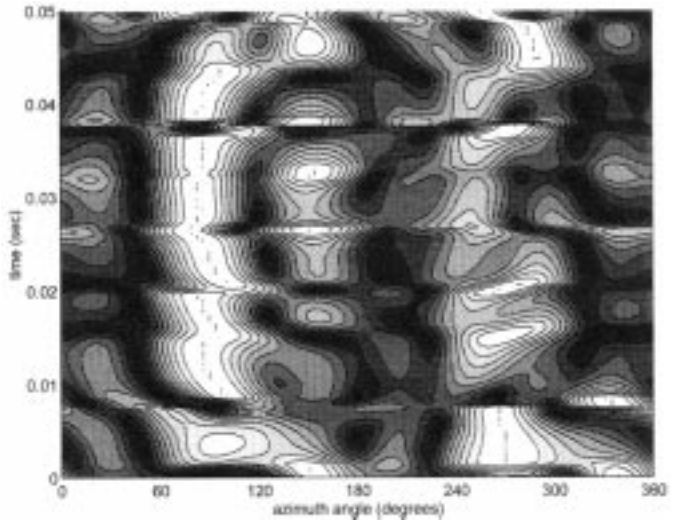

Fig. 15. Directivity pattern (contour plot) at carrier frequency *versus* time for receiver matched to simulated channel.

at azimuth angles near θ_i, $i = 0, 1, 2$ as given above. Note that the lack of strong energy around $\theta_1 = 150°$ comes from the fact that the corresponding path is in a fade at $t = 0.02$ s (see Fig. 13).

Fig. 15 illustrates the variation in time of the DP when the normalized frequency is set to 0 (i.e., carrier frequency for passband equivalent channel). By comparing Figs. 15 to 13, we see that the gain for azimuth angles near θ_i follows closely the magnitude of the channel coefficients. To better analyze the directivity of the simulated channel, we show in Fig. 16 the DPs associated to the channel coefficients of each individual TDP for different values of time. As expected the DPs point toward the mean angle of arrival of the corresponding TDP and the gain associated with each TDP depends on the instantaneous fading conditions. Note that there is no perfect symmetry in the DPs for a given TDP (especially noticeable for the second path). This is due to the fact that the fading correlation between antenna elements is not maximal so that the optimal receiver not only gives a maximum gain in the direction of signal arrival but also gives higher weights to the antenna elements at which the signal exhibit the less fading related attenuation. The DP for the second path exhibit more asymmetry because that TDP has the larger angular spread and is therefore the one for which there is the less fading correlation between antenna elements.

V. Discussion and Conclusion

The numerical complexity of existing vector channel simulators is proportional to the number of TISs. For example, the complexity of the simulator presented in [10] is of order $O(NN_s) + O(NN_e)$, where N is the number of discrete AOA at the base, and N_s is the number of TISs per AOA (which is supposed identical for all values of AOA to simplify the analysis). A transmitted radio-mobile signal in a urban environment is diffracted, refracted and reflected a large number of times, so that the overall propagation process is distributive in nature. The simulation of this distributive process with existing simulators requires that a very large number of discrete AOA be considered. The simulation of a vector channel with existing sim-

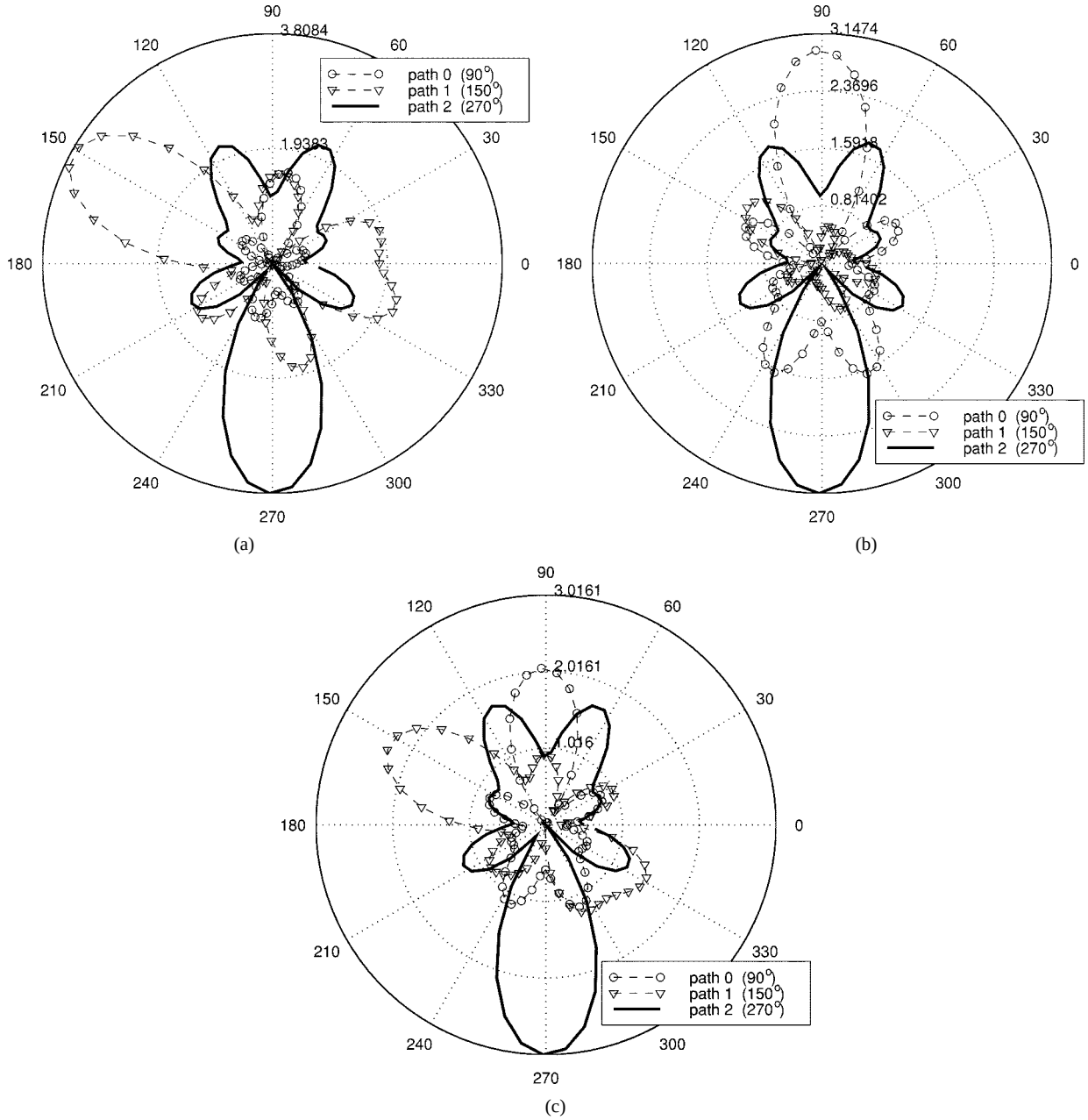

Fig. 16. Path directivity patterns for a receiver match to the simulated channel for three different values of time. (a) $t = 0$. (b) $t = 0.02s$. (c) $t = 0.05s$.

ulators can therefore become very computationally expensive. The new vector channel simulator presented in this paper bypass the need to decompose the channel in its TISs by stochastically modeling the channel variations associated with the combination of these time-varying TISs. The numerical complexity of this new simulator is of order $O(N_e^2 M)$ and is therefore independent of the number of TISs.

The observations presented in the previous section and others made on similar channel realizations obtained for different simulation scenarios lead us to the conclusion that the new simulator is an attractive working alternative to existing vector channel simulators. The new simulator is easy to use and models realistic channel behavior while having a complexity proportional to the number of TDPs, regardless of the number of TISs. This simulator is being used at INRS-Télécommunications to compare the performance of many CDMA receiver algorithms under time-varying conditions. Part of this work has been presented in [28].

APPENDIX A
CHANNEL MODEL DERIVATION

The signal propagation through a single path, from the mobile to the jth antenna element at the base, can be modeled by the following impulse response:

$$h_j(t,u) = \alpha\delta(t - u - \Delta_j(u)) \tag{30}$$

where

t	observation time at the channel output;
u	time at which the impulse is applied at the input;
α	received amplitude;

$\Delta_j(u)$ transmission delay of a signal transmitted at time u, and received at the jth antenna element.

Assuming that the Doppler angle ψ is time-invariant over the observation interval, we have

$$\Delta_j(u) = \Delta_j(0) - \frac{1}{c} uv \cos\psi. \tag{31}$$

Denoting the transmitted signal by $b(t)$, the received signal at the jth antenna element (assuming there is no noise) can therefore be written as

$$w_j(t) = \int_{-\infty}^{\infty} h_j(t,u) b(u)\, du \tag{32}$$

$$= \frac{\alpha}{1-\frac{v}{c}\cos\psi} b\left(\frac{t-\Delta_j(0)}{1-\frac{v}{c}\cos\psi}\right) \tag{33}$$

which, since $v/c \ll 1$, is equal (approximately) to

$$w_j(t) = \alpha b\left(\frac{t-\Delta_j(0)}{1-\frac{v}{c}\cos\psi}\right). \tag{34}$$

We can write $b(t) = z(t)e^{j\omega_c t}$, where $z(t)$ is the baseband equivalent of the transmitted signal, so that

$$w_j(t) = \alpha z\left(\frac{t-\Delta_j(0)}{1-\frac{v}{c}\cos\psi}\right) \exp\left\{ j\omega_c \left(\frac{t-\Delta_j(0)}{1-\frac{v}{c}\cos\psi}\right)\right\} \tag{35}$$

which, assuming $|t-\Delta_j(0)| \ll c/(Bv)$, is equal (approximately) to

$$w_j(t) = \alpha z(t-\Delta_j(0)) \exp\left\{ j\omega_c \left(\frac{t-\Delta_j(0)}{1-\frac{v}{c}\cos\psi}\right)\right\}. \tag{36}$$

We define $\tau = \Delta_0(0)$ and $\rho_j = \Delta_j(0) - \tau$. Under the narrowband array assumption we have $|\rho_j| \ll (1/B)$, so that

$$w_j(t) = \alpha z(t-\tau) \exp\left\{ j\omega_c \left(\frac{t-\tau-\rho_j}{1-\frac{v}{c}\cos\psi}\right)\right\}. \tag{37}$$

Furthermore, by making a Taylor expansion of the argument of the exponential function we can write

$$w_j(t) = \alpha z(t-\tau) \cdot \exp\left\{ j\omega_c t\left(1+\frac{v}{c}\cos\psi + \mathcal{O}_1\left(\frac{v^2}{c^2}\right)\right) - j\omega_c(\tau+\rho_j)\left(1+\mathcal{O}_2\left(\frac{v}{c}\right)\right)\right\} \tag{38}$$

where $\mathcal{O}_i(x)$ represents a term which goes to zero much faster than x. Assuming $t \ll c^2/(f_c v^2)$ and $(\tau+\rho_j) \ll c/(f_c v)$, we therefore have

$$w_j(t) = \alpha e^{-j\omega_c\rho_j} e^{j(\omega_c+\omega_d\cos\psi)t} e^{-j\omega_c\tau} z(t-\tau). \tag{39}$$

The baseband equivalent of the received signal at the jth antenna element is then

$$r_j(t) = \alpha e^{-j\omega_c\rho_j} e^{j(\omega_d t\cos\psi - \omega_c\tau)} z(t-\tau) \tag{40}$$

and the baseband equivalent of the N_e-dimensional vector channel impulse response is

$$\mathbf{h}(t,u) = \alpha e^{j(\omega_d t\cos\psi - \omega_c\tau)} \delta(t-u-\tau)\mathbf{v} \tag{41}$$

where $\mathbf{v}$ is the array propagation vector for the considered path, which is defined as

$$\mathbf{v} = [1, e^{-j\omega_c\rho_1}, \ldots, e^{-j\omega_c\rho_{N_e-1}}]^T. \tag{42}$$

Considering a more realistic propagation scenario for which M TDPs exist, we have

$$\mathbf{h}(t,u) = \sum_{i=0}^{M-1} \delta(t-u-\tau_i)\mathbf{a}_i(t) \tag{43}$$

where

$$\mathbf{a}_i(t) = \sum_{k=0}^{N_i} \alpha_{ik} e^{j(\omega_d t\cos\psi_{ik} - \omega_c\tau_{ik})}\mathbf{v}_{ik} \tag{44}$$

and the indexes ik are used to refer to the variables associated with the kth of the N_i TISs for the ith TDP.

Appendix B
Complex Path Vectors Correlation

From (8) and (2), we obtain

$$\mathbf{R}_{ij}(t,t-\Delta t) \triangleq E\left[\mathbf{a}_i(t)\mathbf{a}_j^H(t-\Delta t)\right] \tag{45}$$

$$= E\left[\int_{\mathcal{T}_i} d\tau \int\int d\theta\, d\psi \alpha(\theta,\psi,\tau) \times \mathbf{v}(\theta) e^{j(\omega_d t\cos\psi - \omega_c\tau)} \times \int_{\mathcal{T}_j} d\tau' \int\int d\theta' d\psi' \alpha^*(\theta',\psi',\tau') \times \mathbf{v}^H(\theta') e^{-j(\omega_d(t-\Delta t)\cos\psi' - \omega_c\tau')}\right] \tag{46}$$

$$= \int_{\mathcal{T}_i} d\tau \int_{\mathcal{T}_j} d\tau' \int\int\int\int d\theta\, d\psi\, d\theta'\, d\psi' \mathbf{v}(\theta)\mathbf{v}^H(\theta') \times E[\alpha(\theta,\psi,\tau)\alpha^*(\theta',\psi',\tau')] e^{j\omega_d\Delta t\cos\psi'}. \tag{47}$$

Then, from (4), (5), and the fact that the power density function with respect to the Doppler angle, ψ, is uniform, we get

$$\mathbf{R}_{ij}(t,t-\Delta t) = \delta_{ij}/\pi \int_0^{\pi} e^{j\omega_d\Delta t\cos\psi}\, d\psi \times \int_{\mathcal{T}_i} f_a(\tau)\, d\tau \int f_c(\theta;i)\mathbf{v}(\theta)\mathbf{v}^H(\theta)\, d\theta \tag{48}$$

$$= \delta_{ij} J_0(\omega_d\Delta t) F_a(i) \mathbf{R}_{\mathbf{v},i} \tag{49}$$

which is the desired result.

References

[1] D. B. Woerner, J. H. Jeffrey, and T. S. Rappaport, "Simulation issues for future wireless modems," *IEEE Commun. Mag.*, pp. 42–53, July 1994.

[2] A. J. Paulraj and C. B. Papadias, "Space-time processing for wireless communications," *IEEE Signal Processing Mag.*, vol. 14, no. 6, pp. 49–83, Nov. 1997.

[3] B. H. Khalaj, A. Paulraj, and T. Kailath, "2D RAKE receivers for CDMA cellular systems," in *Proc. IEEE Global Commun. Conf.*, San Francisco, CA, Dec. 1994, pp. 1–5.
[4] R. Kohno, P. B. Rapajic, and B. S. Vucetic, "An overview of adaptive techniques for interference minimization in CDMA systems," in *Wireless Personal Communication*. Norwell, MA: Kluwer, 1994, pp. 3–21.
[5] A. F. Naguib and A. Paulraj, "Performance of DS/CDMA with M-ary orthogonal modulation cell site antenna arrays," in *Proc. ICC'95*, Seattle, WA, June 1995, pp. 697–702.
[6] M. Nagatsuka and R. Kohno, "A spatially and temporally optimal multi-user receiver using an array antenna for DS/CDMA," *IEICE Trans. Commun.*, vol. E78-B, no. 11, pp. 1489–1497, Nov. 1995.
[7] J. Ramos and M. Zoltowski, "Blind 2D RAKE receiver for CDMA incorporating code synchronyzation and multipath time delay estimation," in *Proc. ICASSP'97*, Apr. 1997, pp. 4025–4027.
[8] J. Thompson, P. Grant, and B. Mulgrey, "Asymptotic performance of blind antenna array receiver algorithms for CDMA," in *Proc. ICASSP'97*, Apr. 1997, pp. 4017–4020.
[9] C. Vaidyanathan and K. Buckley, "An adaptive decision feedback equalizer antenna array for multiuser CDMA wireless communications," in *Proc. 30th Asilomar Conf. Signals, Systems, and Computers*, Nov. 1996, pp. 340–344.
[10] G. Rayleigh, S. N. Diggavi, A. F. Naguib, and A. Paulraj, "Characterization of fast fading vector channels for multi-antenna communication systems," in *Proc. 29th Asilomar Conf. Signal, Systems, and Computers*, Nov. 1995, pp. 853–857.
[11] G. L. Turin, "Introduction to spread-spectrum antimultipath techniques and their application to urban digital radio," *Proc. IEEE*, vol. 68, no. 3, pp. 328–353, Mar. 1980.
[12] T. Jämsä, T. Poutanen, and H. Hakalahti, "Realization of a multipath radio channel simulator for wideband wireless radio systems," in *Proc. Viginia Tech 7th Symp. Wireless Personal Commun.*, June 1997, pp. 2-1–2-11.
[13] G. J. R. Povey, P. M. Grant, and R. D. Pringle, "A decision-directed spread-spectrum RAKE receiver for fast-fading mobile channels," *IEEE Trans. Veh. Technol.*, vol. 45, no. 3, pp. 491–502, Nov. 1996.
[14] H. Krim and M. Viberg, "Two decade of array signal processing research," *IEEE Signal Processing Mag.*, pp. 67–94, July 1996.
[15] *The Mobile Communications Handbook*, J. D. Gibson, Ed., CRC Press, Boca Raton, FL, 1996, pp. 430–447. CDMA technology and the IS-95 north American standard.
[16] W. C. Jakes, *Microwave Mobile Communications*. New York: Wiley, 1974.
[17] S. Haykin, *Adaptive Filter Theory*, 3rd ed. Englewood Cliffs, NJ: Prentice-Hall, 1996.
[18] A. F. Naguib, "Adaptive Antennas for CDMA Wireless Network," Ph.D. dissertation, Stanford University, Stanford, CA, 1996.
[19] M. D. Yacoub, *Foundations of Mobile Radio Engineering*. Boca Raton, FL: CRC Press, 1993.
[20] J. I. Smith, "A computer generated multipath fading simulation for mobile radio," *IEEE Trans. Veh. Technol.*, vol. 24, no. 3, pp. 39–40, Aug. 1975.
[21] A. Papoulis, *Probability, Random Variable, and Stochastic Processes*, 2nd ed. New York: McGraw-Hill, 1984.
[22] D. G. Luenberger, *Introduction to Linear and Nonlinear Programming*. Reading, MA: Addison-Wesley, 1989.
[23] B. Picinbono, *Random Signals and Systems*. Englewood Cliffs, NJ: Prentice-Hall, 1993.
[24] S. Valaee, B. Champagne, and P. Kabal, "Parametric localization of distributed sources," *IEEE Trans. Signal Processing*, vol. 43, no. 9, pp. 2144–2153, Sept. 1995.
[25] R. G. Keys, "Cubic convolution interpolation for digital image processing," *IEEE Trans. Acoust., Speech, Signal Processing*, vol. 29, no. 6, pp. 1153–1160, Dec. 1981.
[26] A. V. Oppenheim and R. W. Schafer, *Discrete-Time Signal Processing*. Englewood Cliffs, NJ: Prentice-Hall, 1989.
[27] *The Mobile Communications Handbook*, J. D. Gibson, Ed., CRC Press, Boca Raton, FL, 1996, pp. 166–176. Diversity Techniques.
[28] A. Stéphenne and B. Champagne, "Convergence properties of blind algorithms for base station CDMA receivers," in *Proc. ICASSP'98*, Seattle, WA, May 1998, pp. VI.3181–VI.3184.

Alex Stéphenne was born in Quebec, Canada, on May 8, 1969. He received the B.Ing. degree in electrical engineering from McGill University, Montreal, Quebec, in 1992, and the M.Sc. degree and Ph.D. degrees in telecommunications from INRS-Télécommunications, Université du Québec, Montreal, in 1994 and 1999, respectively.

He is currently as a DSP Design Specialist for Dataradio Inc., Montreal, a company specializing in the design and manufacturing of advanced wireless data products and systems for mission critical applications.

Benoît Champagne was born in Joliette, Quebec, Canada, on January 13, 1961. He received the B.Ing. degree in engineering physics from the Ecole Polytechnique of Montréal in 1983, the M.Sc. degree in physics from the University of Montreal in 1985, and the Ph.D. degree in electrical engineering from the University of Toronto, Toronto, Ontario, Canada, in 1990.

From 1990 to 1999, he was with INRS-Télécommunications, Université du Québec, Montreal, Canada, first as an Assistant Professor, and from 1995 on, as an Associate Professor. In September 1999, he joined McGill University, Montreal, Quebec, Canada, as an Associate Professor with the Department of Electrical and Computer Engineering. He remains a Visiting Professor at INRS. His current research interests include statistical signal processing, sensor array processing adaptive filtering, and applications thereof in telecommunication engineering.